J Mater Sci (2007) 42:1682–1693
DOI 10.1007/s10853-006-0974-y

Deformed metals and alloys with a structural scale from 5 nm to 100 nm

H. W. Zhang · N. Hansen

Received: 28 June 2006 / Accepted: 15 September 2006 / Published online: 9 January 2007

Abstract The processing, structure and properties of deformed metals and alloys with a structural scale from the micrometer to the nanometer dimensions has been the subject of a recent viewpoint set [1]. The present paper will focus on deformed metals and alloys with a structural scale from 5 nm to 100 nm, concentrating on materials processed by high pressure torsion (HPT), surface mechanical attrition treatment (SMAT) and sliding. A detailed microstructural characterization has been followed by an analysis of the relationship between structural features and processing parameters. In this analysis, some general approaches have been applied for example scaling of the evolution of the boundary spacing. This analysis is the basis for a brief discussion of the relationship between the microstructural parameters and the strength.

Introduction

The grain refinement of ductile materials by means of plastic deformation has initiated extensive research in the past decade. The structural refinement covering many length scales encompasses traditional metals with a length scale in the micrometer/submicrometer range and nanostructured metal with a length scale below 100 nm. Some processes such as equal channel angular extrusion (ECAE) [2], multiple forging [2], cyclic extrusion compression [3] and accumulative roll bonding (ARB) [4] can refine grains into the submicron scale. However, high pressure torsion (HPT) [2], sliding [5], ball milling [6], shot peening [7] and surface mechanical attrition treatment (SMAT) [8–12] have the potential to produce nanostructures with a scale of 5–100 nm in the form of bulk samples, powders and surface layers. The nanoscale materials have been the subject of one viewpoint set [13], whereas metals and alloys with a structural scale from the micrometer to the atomic dimension have been covered in another [1]. The present paper will focus on deformed metals and alloys with a structural scale from 5 nm to 100 nm processed by the three deformation routes: high pressure torsion (HPT), surface mechanical attrition treatment (SMAT) and sliding/friction.

Processing

HPT is a well-known technique that can produce nanometer scale structure in bulk metals [2, 14–17]. A disk shaped sample (0.2–1.0 mm in thickness and 10–15 mm in diameter) is subjected to torsion deformation under a high hydrostatic pressure of the order of several GPa (see Fig. 1a). The strain rate is low for example 0.7–17 s^{-1} [14]. The shear strain produced by HPT varies linearly from zero in the center to the maximum value at the rim of the disk. The amount of shear strain depends on the thickness of the sample and the number of rotations [2]. Strain–microstructure relationships can be obtained by sampling from different positions along the diameter of the disc.

H. W. Zhang (✉) · N. Hansen
Center for Fundamental Research: Metal Structures in Four Dimensions, Materials Research Department, Risø National Laborabory, Frederiksborgvej 399, 4000 Roskilde, Denmark
e-mail: hwzhang2001@yahoo.com.cn

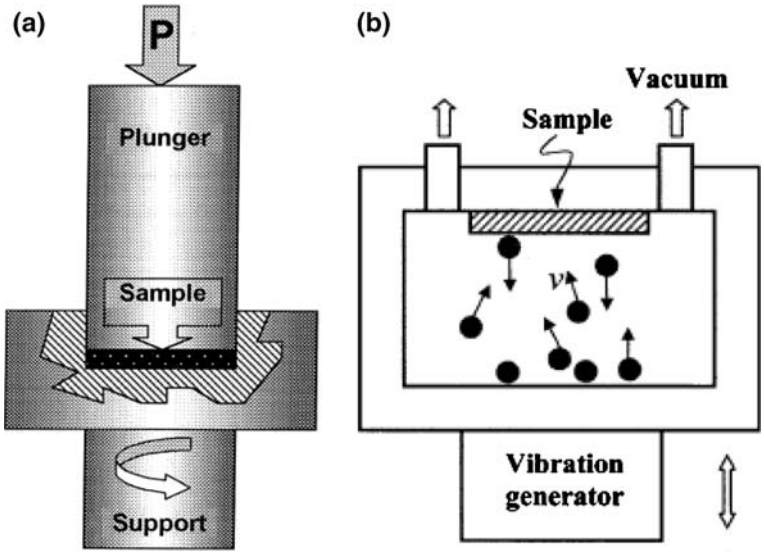

Fig. 1 Schematic illustrations of processing by HPT (**a**) [17] and SMAT (**b**) [10]

SMAT is a relatively new technique which has been developed in order to achieve large plastic deformation at a sample surface [8]. As shown in Fig. 1b, SMAT is carried out in a cylinder shaped vacuum chamber containing steel balls of 1–10 mm in diameter with a smooth surface. The chamber is connected to a high frequency generator (frequency 50 Hz to 20 kHz) resonating the steel balls which in turn deform the sample surface by shot blasting in random directions. The velocity of the shots is estimated to be 1–20 m s^{-1} giving a high strain rate of the order of 10^2–10^3 s^{-1}, which is controlled by a number of processing parameters e.g. vibration frequency, ball diameter and traveling distance of the balls [8]. The temperature rise during the treatment is affected by the material characteristics and the impact intensity for example in a Fe sample the temperature rise has been estimated to be the order of 50–100 °C [8]. SMAT is similar to traditional surface treatment techniques e.g. shot peening. A difference is however the use of large diameter smooth balls in SMAT compared with smaller shots (0.1–1 mm in diameter) of irregular shape in shot peening. The increase in the diameter of the balls increases the thickness of the nanostructured surface layer. This effect is however counterbalanced by the much smaller velocity of the balls in SMAT compared to shot peening, where a typical speed is 100 m s^{-1}. By means of SMAT, graded microstructure has been produced as shown in Fig. 2 for Cu (K. Wang et al., unpublished), Fe [10] and an Al-alloy [11]. The graded structure is formed due to a continuous decrease in strain and strain rate with increasing distance from the surface. By optimizing the process conditions nanostructured surface layer with a thickness up to 50 μm can be produced both in pure metals [K. Wang et al., unpublished, 10] and in alloys [9, 11, 12].

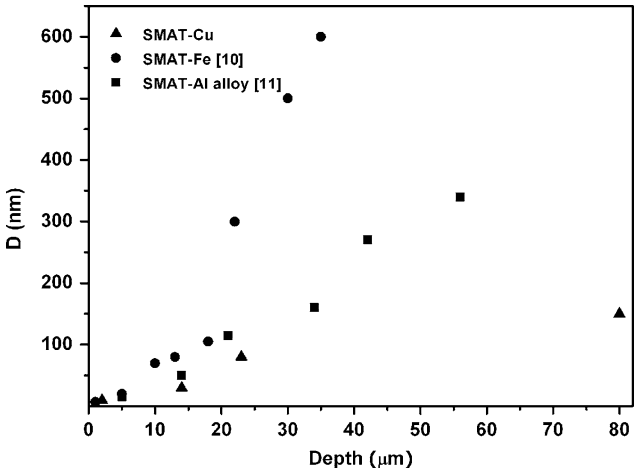

Fig. 2 The variations in boundary spacing (D) with depth in Cu (K. Wang et al., unpublished data), Fe [10] and an Al-alloy [11] deformed by SMAT

Sliding deformation is selected to simulate friction and wear. Scientifically, it has been used to follow the evolution of a nanostructure in soft copper sliding against steel in a flat plate friction tester [5, 18]. The steel is in the form of a slider (platen) which has been ground to produce ridglike asperities with a wavelength of 130 μm and a 5–10° inclination angle. Two hydraulic pistons on each side of the platen apply a normal force (10–20 MPa) to two copper samples forming a copper–steel–copper sandwich. The platen is attached to a servo-hydraulic machine which controls the sliding speed and distance and measures the sliding

force. In the actual experiment [5, 18], the sliding speed has been set to 0.25 and 25 mm s^{-1} and the sliding distance to 120 mm, which produces a strain rate < 10 s^{-1}. A structural characterization has shown the formation of a graded deformation microstructure covering a scale from 5 nm to 10 nm in the surface layer to a submicrometer dimension in a depth of more than 10 μm [5, 18]

The three kinds of deformation techniques outlined above can refine structures into the nanometer scale (5–100 nm). The strain for all the processes can reach extremely high levels for example by increasing the number of rotations in HPT and by increasing the treatment time in SMAT. All these processes produce graded structures from a micro/submicrometer scale to a nanometer scale being the results of large strain and strain gradients. Such graded structures allow in one sample the examination of the microstructural evolution from small to large strain. The strain rate in these techniques is different: (i) In HPT the rate is about 0.7–17 s^{-1} (estimated based on the parameters in [14]) (ii) In sliding the rate is <10 s^{-1} (estimated based on the parameters in [5, 18], (iii) in SMAT the rate is 10^2–10^3 s^{-1} [8]. Additionally, the deformation in HPT and sliding is basically monotonic shear deformation that is different from the random changeable deformation directions during SMAT. This difference may lead to the formation of equiaxed grains in SMAT [8–12] compared with the typical lamellar structures for example observed in HPT Ni [14, 15] and slided Cu [5, 18]. From the point of industrial application, all techniques have limitations for example in HPT an inhomogeneous structure in a small sample, in sliding a relatively thin surface layer and in SMAT the requirement of a regular sample shape e.g. a plate shaped sample.

Structural evolution

During plastic deformation the microstructure evolves in a continuous manner from the micrometer to the nanometer scale [5, 14, 19–21]. Although this paper will focus on the microstructure on a scale of less than 100 nm, the structural evolution on a larger scale will be briefly summarized below.

The microstructural evolution for metals of medium to high stacking fault energy (SFE) and of low SFE has been classified in detail [21]. In [21] a glossary of structural features and nomenclature is included, which will be the basis of the structural characterization in the following. A central point is the separation of subdividing boundaries according to the mechanisms by which they are formed into geometrically necessary boundaries (GNBs) and incidental dislocation boundaries (IDBs). GNBs are formed by different slip activities on each side of the boundaries, and IDBs develops by statistical trapping of dislocations [22]. GNBs include dense dislocation walls, double walled microbands and lamellar boundaries. GNBs are extended boundaries which have a specific 3D-orientation with respect to the axes of the crystallographic lattices as well as to the macroscopic deformation axes of the sample. IDBs are short and randomly inclined cell boundaries.

The structural classification in [21] differentiates between medium to high SFE metals with easy 3D mobility of dislocations and low SFE metals with restricted dislocation mobility. In the former group the structure is subdivided by dislocation boundaries and high angle boundaries in a 3D structure with a relatively small density of dislocations between the boundaries. In the latter group extended planar boundaries (GNBs) form and between the boundaries the dislocations arrange in a fairly uniform pattern, the so-called Taylor lattice [23, 24]. For both groups the deformation takes place by slip which for the low SFE metals is supplemented by twinning. Typically examples of the two types of structures are shown in Fig. 3a, b for a high stacking fault energy metal (Al) and a low stacking fault energy alloy (AISI 304 stainless steel). In the 10% cold-rolled polycrystalline Al (Fig. 3a) [25], the GNBs are the extended boundaries marked by A, B, C, etc., for which also the misorientation angle is shown. Short random cell boundaries (IDBs) marked a, b, c. etc. are observed between the extended boundaries forming typical cell blocks marked CB_1, CB_2, CB_3, etc. In the AISI 304L stainless steel deformed at room temperature by compression (Fig. 3b) [26], dislocation boundaries, deformation twins, and a strain-induced martensite phase are observed. The dislocations are more or less uniformly distributed between the planar GNBs, forming a multiple-Burgers-vector Taylor lattice [22].

The subdivision of the coarse grains by GNBs and IDBs during deformation changes with increasing strain and stress, typically the spacing of GNBs and IDBs decreases and the misorientation angle across the boundaries increases [25–28]. Figure 4a, b shows the variations of the GNB spacing and the boundary misorientation angle, respectively, with strain in a commercial purity aluminum deformed from ε_{vM} = 1.6–6.4 (ε_{vM}: von Mises strain) by conventional cold-rolling and ARB [20]. The boundary spacing decreases to about 240 nm (Fig. 4a) and the boundary misorientation angle increases to about 36° (Fig. 4b) at the largest strain applied [20].

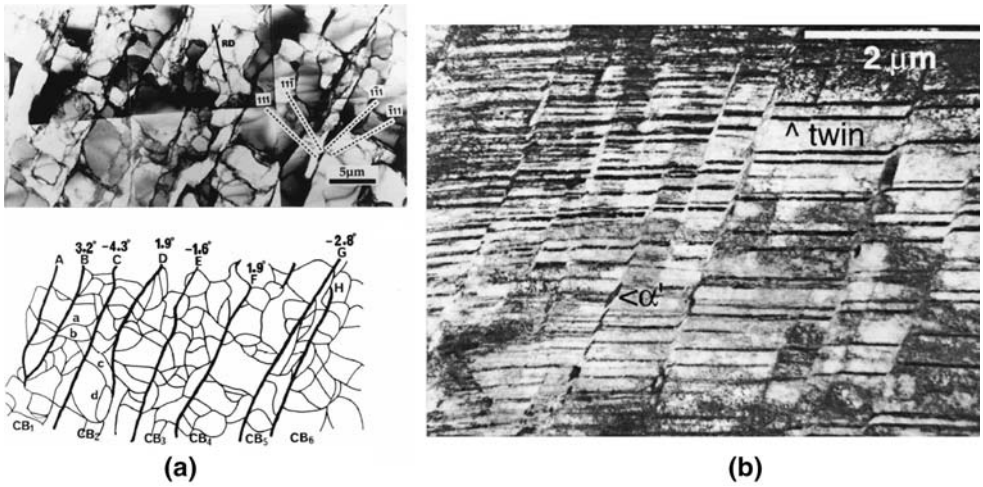

Fig. 3 (**a**) Typical deformation structures in pure Al (99.996% purity) deformed by cold-rolling to a thickness reduction of 10% [25] and (**b**) AISI 304L stainless steel deformed by compression (ε_{vM}: von Mises strain = 5) [26]. In (**a**), the rolling direction (RD) is marked by an arrow and the traces of {111} planes are marked by dashed lines. The GNBs form cell blocks subdivided by IDBs. In (**b**) Taylor lattice, dislocation boundaries, intersecting deformation twins and deformation induced martensite (α') are observed

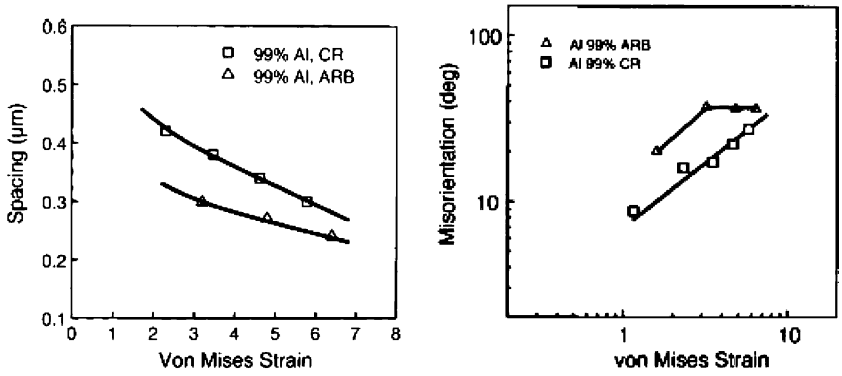

Fig. 4 The boundary spacing (**a**) and boundary misorientation angle (**b**) as a function of ε_{vM} in commercial purity (99%) aluminum samples deformed by conventional cold-rolling and ARB [20]

The grain subdivision process by formation of dislocation boundaries continues into the nanometer regime (below 100 nm). The monotonic HPT-deformation introduces a structure consisting of extended planar boundaries and interconnecting short boundaries similar to structures observed after conventional rolling and drawing. In order to characterize such structures in detail, the choice of the observation plane is important as discussed in [14]. This is demonstrated for Ni by the observation of an equiaxed structure in the torsion plane [14, 29] compared to a well defined lamellar structures observed in a plane perpendicular to the torsion plane (the longitudinal plane), see Fig. 5a. This plane contains the maximum shear directions and it is found that two sets of extended boundaries subdivide the structure (see Fig. 5b). One set is parallel to the shear direction and the other set is inclined with a large angle to the shear direction. Both of the traces of the boundaries are very close to the trace of (111) [14]. Deformation twins of nanometer dimensions are observed in a sample deformed to a large strain $\varepsilon_{vM} > 5.0$ (see Fig. 5c [14]. Such twins are not normally found in deformed Ni as the critical shear stress for twin formation is very large in this high stacking fault energy metal. This critical shear stress may be about 300 MPa [30] or even much higher than 500 MPa [14]. However, as the structural scale refines with increasing strain, the yield stress of HPT-deformed Ni is estimated to increase to 800 MPa or higher [16], which may surpass the critical stress for twin formation. The deformation twins therefore become a part of the deformation process when the grain size decreases into the nanometer range, which agrees with experimental observations [31–37] as well as with molecular dynamic simulations [38–41]. The structural refinement at large strain may therefore be a result of a slip and some additional twinning.

The structural refinement by sliding deformation has been discussed in detail [5] and only a brief summary is

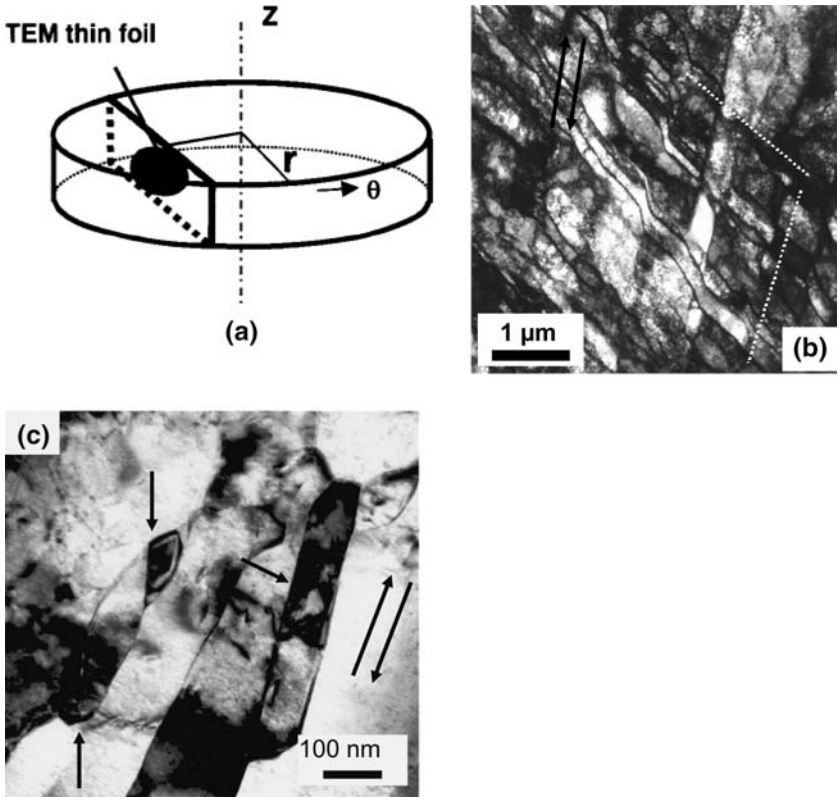

Fig. 5 Dislocation microstructures observed by TEM in pure Ni (99.99% purity) deformed by HPT to $\varepsilon_{vM} = 12$. The observed plane (longitudinal section) is shown in (**a**) where Z is the torsion axis, r is the radius and θ is the shear direction. The microstructure is shown in (**b**) where two sets of extended boundaries are seen (marked by dotted lines). The shear directions are marked by double arrows. The microstructure in a high magnification is shown in (**c**) where deformation twins are marked with arrows [14, 15]

given in the following. A typical structure is illustrated in Fig. 6a, showing a graded nanostructure with extended boundaries (GNBs) almost parallel to the sliding surface. The average perpendicular spacing D_{av}^{GNB} of the boundaries increase with increasing depth, as shown in Fig. 6b, from about 10 nm near the surface to about 80 nm at 4 μm below the surface. This spacing is of the same order as the spacing (~130 nm) in Ni cold rolled to a reduction of 98% in thickness [42]. With increasing strain the structural refinement is followed by an increase in the average misorientation angle across the boundaries and in the density of high angle boundaries. However, although most of the boundaries are of high angle, the interior dislocation density is high. This density has been estimated to be of 10^{16} m^{-2} [5, 26] which is one to two orders larger than that typically observed in metals cold rolled to a large strains.

Deformation by SMAT will be described briefly for metals with different crystallographic structures (i) Fe (b.c.c.) [10]; (ii) AISI 304 stainless steel (f.c.c.), [9]; (iii) Ti (h.c.p.) [12].

Iron is a typical b.c.c. metal which deforms by dislocation slip [10]. Deformation by SMAT introduces a graded structure in the sample with a boundary spacing of about 7 nm at the surface (Fig. 7a, b) which increases to about 100 nm in a depth of 15 μm (Fig. 7c) [10]. In the deep layers of low strain deformation, cross-sectional TEM observations show a typical grain subdivision by dislocation boundaries e.g. dense dislocation walls (DDWs) and dislocation tangles (DTs). As the surface is approached the average misorientation angle increases, the boundary spacing decreases and an equiaxel structure replaces the elongated structure.

AISI 304 stainless steel is a f.c.c. metals with a low stacking fault energy (SFE) approximately

Fig. 6 (**a**) Cross-sectional TEM observations of the graded dislocation structures and (**b**) the variation of average spacing of extended boundaries (D_{av}^{GNB}) with depth in a copper sample deformed by sliding. The sale bar in (**a**) is 2 μm [5]

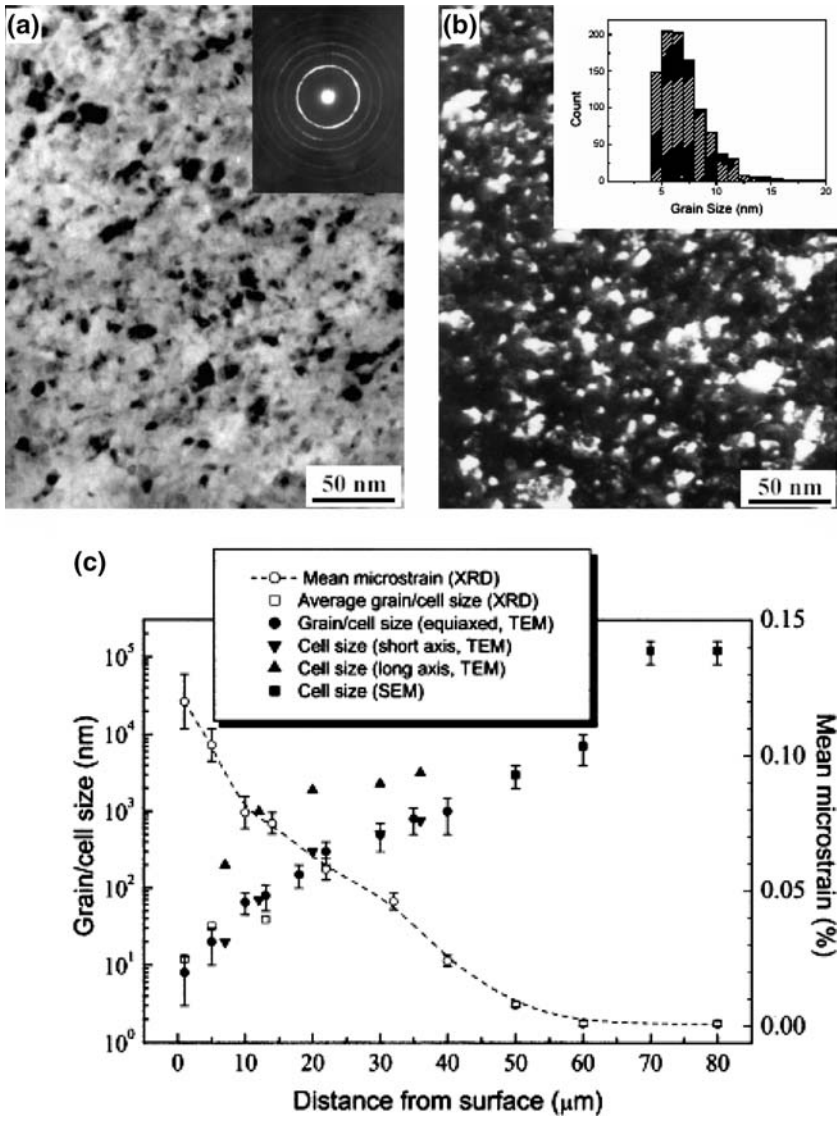

Fig. 7 TEM observations of the microstructures in pure Iron (99.95% purity) deformed by SMAT for 60 min in vacuum. The microstructure is shown in (**a**) as a bright field image and in (**b**) as a dark field image of the surface layer. In (**a**) the inserted selected area diffraction pattern indicates a random distribution of the grain orientations. In (**b**) the inserted grain size distribution in the surface layer reveals a logarithmic distribution with an average grain size about 7 nm. In (**c**) is plotted the grain/cell size and the mean microstrain as a function of the depth below the surface [10]

17 mJ m^{-2}[9]. In this metal, SMAT has produced a graded structure with a boundary spacing of about 10 nm at the surface and 60 nm in a depth of 30 μm below the surface (see Fig. 8) [9]. Cross-sectional microscopy has confirmed that mechanical twins dominate the structure together with features being a result of a phase transformation [9]. In general, the formation of mechanical twins introduces twin boundaries that can be viewed as a $60^\circ\langle 111\rangle$ twist boundary or a $70.5^\circ\langle 110\rangle$ tilt boundary. Therefore, the formation of twins introduces high-angle boundaries which subdivide the structure. Additionally, twin–twin intersections can result in a martensite transformation which takes place at intersection points. The martensite transformation introduces phase boundaries which subdivide the structures. Figure 9a, b shows a typical microstructure with twins and martensite. This kind of grain subdivision by twin boundaries and phase boundaries follows a similar path with increasing strain as observed for dislocation boundaries, i.e. the spacing of the twins decreases and their density increases as the surface is approached [9].

Titanium is a typical h.c.p. metal which deforms by a combination of slip and twinning [12]. In this material, SMAT has introduced a graded structure subdivided by dislocation boundaries and high angle (twin) boundaries. For example a typical structure observed at a depth of 15–30 μm shows mean boundary spacing of about 150 nm, see Fig. 10 [12].

In conclusion, the microstructural evolution during HPT, SMAT and sliding deformation shows that the grain subdivision is controlled by the formation and evolution of dislocation boundaries and high angle boundaries including twin boundaries. The subdivision

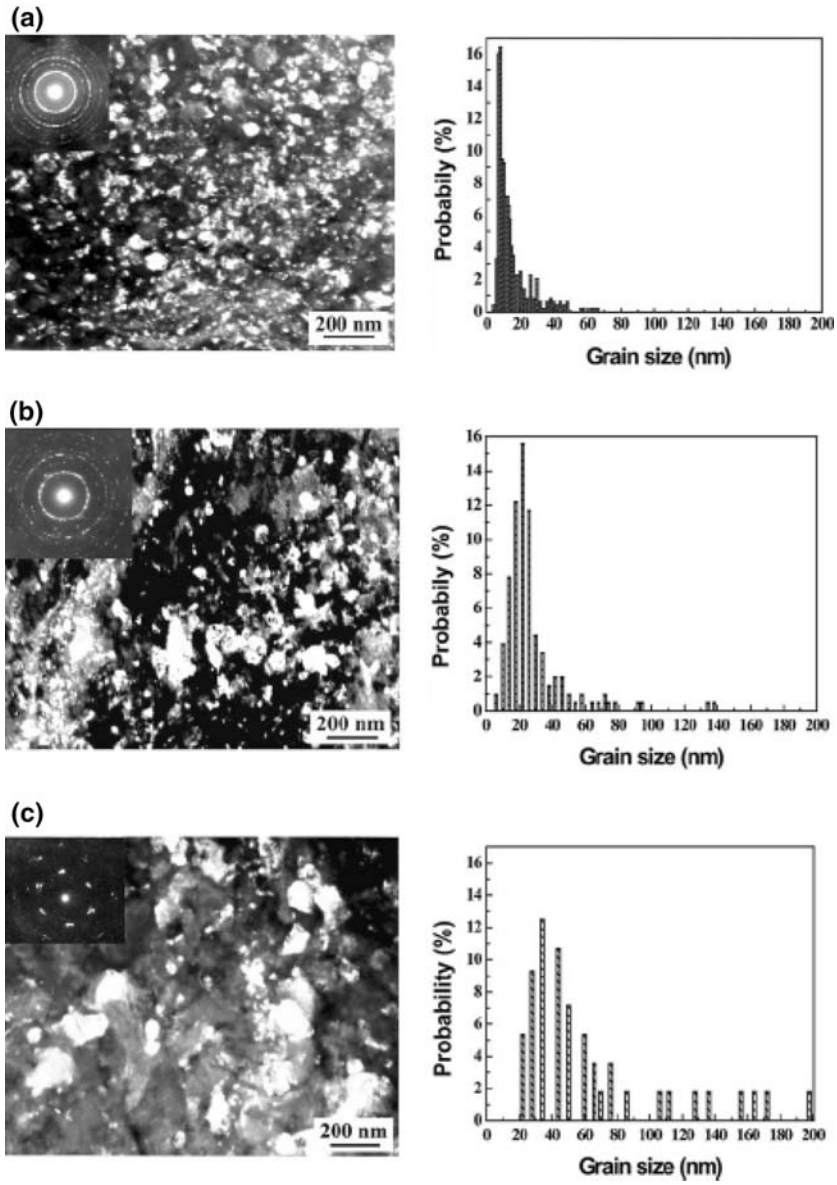

Fig. 8 TEM observations of the microstructure in the AISI 304 stainless steel deformed by SMAT for 15 min in vacuum [9]. The microstructure is shown in dark field images: (**a**) at the surface and (**b**) at a distance of 15 μm below the surface and (**c**) at a distance of 30 μm below the surface. The grain size (boundary spacing) distribution is also plotted in this figure

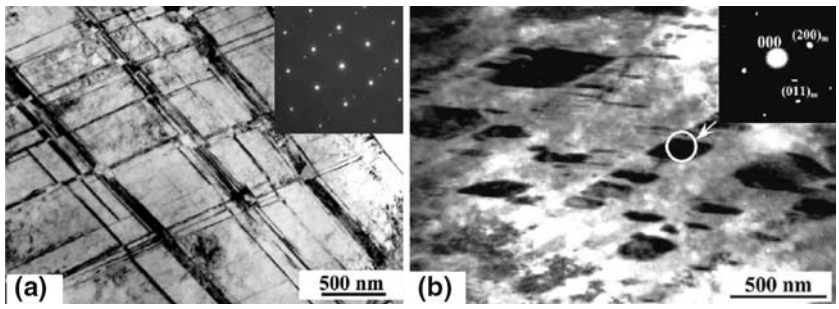

Fig. 9 (**a**) Deformation twins and (**b**) martensite in AISI 304 stainless steel treated by SMAT for 15 min in vacuum [9]. The inserted selected area diffraction patterns (SAED) correspond to: (a) the twin diffraction obtained with the electron beam parallel to ⟨110⟩ and (b) the martensitic phase

is affected by process parameters such as strain, strain rate and deformation mode and material parameters such as SFE and lattice structure. Metals with medium to high SFE follow the general patterns of grain subdivision by two types of dislocation boundaries (GNBs and IDBs) into the nanometer scale. In low SFE f.c.c. metals and h.c.p. metals, mechanical twins also participate in the grain subdivision process, especially pronounced in a high strain rate process as SMAT.

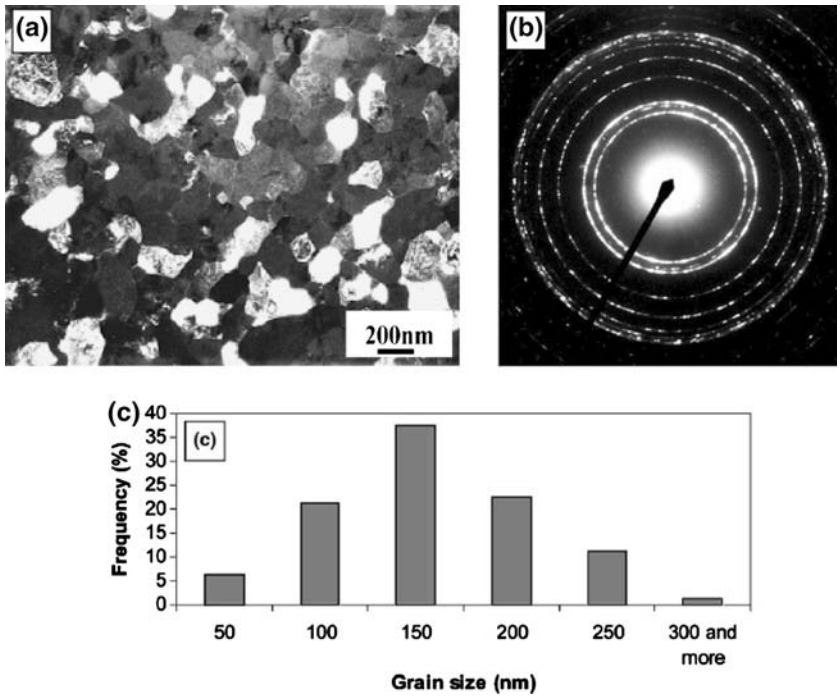

Fig. 10 Commercially pure titanium deformed by SMAT for 60 min in vacuum [12]. The microstructure at a distance of 15–30 μm depth from the surface is exemplified by (**a**) a dark field image (**b**) a selected area diffraction pattern and (**c**) a histogram of the grain size distribution

Structural quantification

Typical structural features in the deformed structure are dislocation boundaries, high angle boundaries, dislocations between boundaries and twins. It is typically observed that the boundary spacing decreases and the misorientation angle increases with increasing strain. An example is large strain deformation by sliding [5, 26] where a boundary spacing as small as 5–10 nm has been measured at the surface [5]. It also appears that the misorientation angle increases with strain in such a way that the fraction of high angle boundaries increases to be of the order of 80% or higher as shown in sliding samples [5]. For all structural scales a significant amount of dislocations are present between boundaries. The dislocation density has been estimated in a HPT sample deformed to a large strain to be the order of 10^{14}–10^{15} m^{-2} [17] and in sliding to be about 10^{16} m^{-2} [5, 26]. Finally twin formation is typically observed in low stacking fault energy metals deformed to medium and large strain, whereas twinning in high stacking fault energy metals as Al, Cu, Ni only is observed in very fine scale structures and is related to the high stress state for such structures.

Quantification of the structural dependency of the boundary spacing (or the surface area per unit volume, S_v) with strain has been suggested for metals deformed in torsion and by cold-rolling, see Fig. 11a. In this log–log plot a linear relationship i.e. a power law is observed however with a higher slope for Ni when compared with Cu and Al. This behavior may be related to the reduced dislocation annihilation in Ni having the highest melting point [26]. The relationship in Fig. 11a has also been used to estimate the strain in a Cu sample deformed by sliding by extrapolating the power law for torsion Cu [43] and rolled Cu [44] using the boundary spacing which has been determined as a function of the depth below the surface for the deformed sample, see Fig. 11b [5]. Based on this figure the strain at the surface is estimated to be over 100 [5]. Recently, a minimum boundary spacing of about 10 nm in pure Ni has been obtained by a repeated rolling and folding technique to a strain of $\varepsilon_{vM} = 64$ [45] A plot of log 64/log 0.1 nm in Fig. 11a agrees reasonably well with the data for sliding. When the spacing data for HPT Ni [14] (under a hydrostatic pressure of 4.0 GPa) is plotted versus the strain, see Fig. 11a, it is found that a linear relationship is observed with a same slope as for cold rolled Ni [42] when the shear strain is smaller than 5.0, whereas above this value a power law with a smaller slope is obtained. In order to estimate the strain level in a SMAT sample the power law for rolled Cu [43] has been extrapolated using the experimental spacing data obtained for SMAT Cu which is shown in Fig. 2 (K. Wang et al., unpublished). The strain data as a function of distance below the surface are shown in Fig. 11c. It is seem that a very high strain level above 400 is reached by SMAT at the surface, with a decrease in strain level to about 10 in a depth of 20 μm and to 1

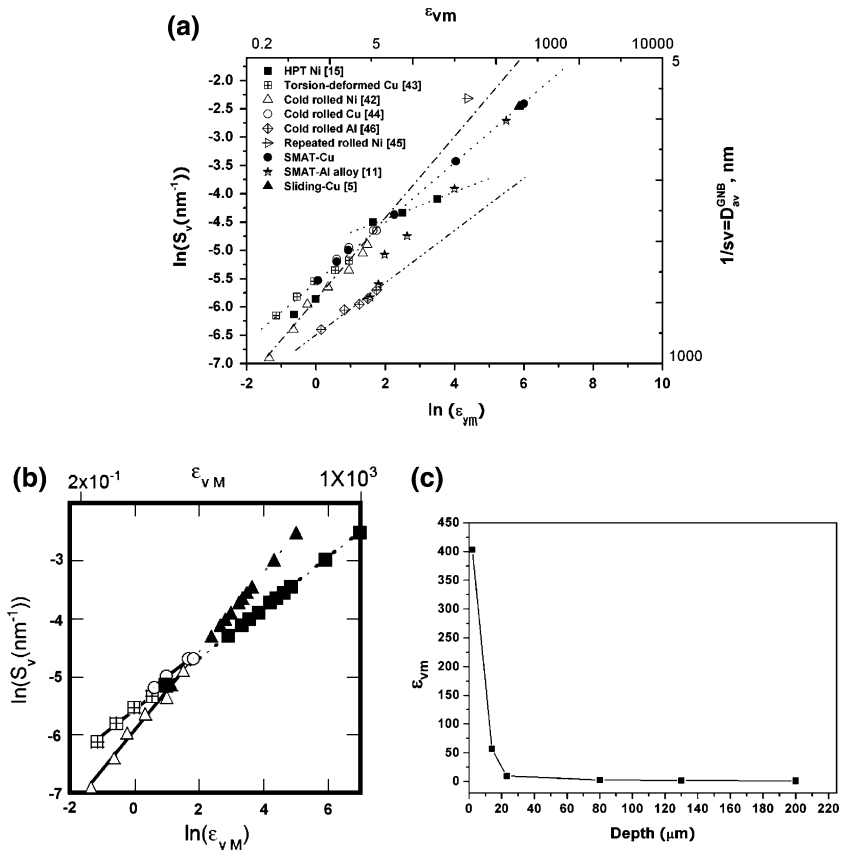

Fig. 11 (**a**) Power law relationship between boundary area per unit volume (S_v) and strain (ε_{vM}) for metals deformed by different techniques. In (**b**) is shown strain extrapolation data (■ and ▲) for Cu deformed by sliding [5] based on experimental data for rolled Ni (Δ) [42], torsion deformed Cu (⊞) [43] and rolled Cu (○) [44]. Based on (**b**) the strain is shown in (**c**) as a function of the depth below the surface of Cu deformed by SMAT

in a depth of 200 μm. By using the strain data of Fig. 11c, the spacing data of the SMAT-Al alloy [11] is also plotted in Fig. 11a. A linear relationship as in rolled Al [46] has been obtained at small to medium strains indicating a comparable structural evolution for these different processes in this strain regime.

In Fig. 11a the only parameter is the strain, and the data have all been obtained by deformation at room temperature at relatively low strain rate for example less than 1–25 s^{-1} in rolling. However, other parameters such as temperature and composition can also play a role. For example elements in solid solution that stabilize the deformation structure may change the relationship between the strain and the spacing. In the surface layer (0–6 μm) in Cu deformed by sliding, about 1% Fe is detected [18], and by SMAT using steel shots, elements such as Fe and O can be introduced.

In the analysis of the evolution of the boundary spacing with increasing strain, it has been suggested to examine the probability distribution of the spacing normalized by the average value [47–49]. This approach has been used to analyses the boundary spacing in layers at increasing distance from the surface in a Cu sample deformed by sliding [5]. Distributions with different average value have been scaled resulting in a single distribution see Fig. 12. This result has been taken as a demonstration of the similarity of the subdivision process taking place at different length scales from the submicrometer to the nanometer range [5, 26]. A similar scaling approach has been applied to the a number of metals deformed by SMAT and one single distribution has been obtained independent of the material type as shown in Fig. 13. The scaling behavior of the spacing distribution holds over nearly three orders of magnitude in the strain level from 0.1 to 100, and over several decades on the length scale.

Microstructure-flow stress

For the three processing techniques discussed above the deformation microstructure contains predominately dislocation boundaries and high angle boundaries where the latter are the original grain boundaries,

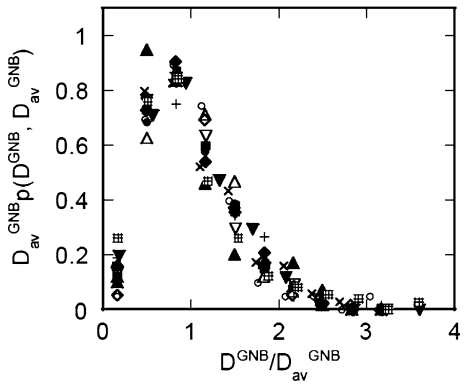

Fig. 12 Probability distributions of nanometer scale boundary spacings normalized by their average spacing in sliding Cu [5] (average GNB spacing: 12 nm (○), 19 nm (□), 31 nm (◇), 35 nm (△), 38 nm (▽), 41 nm (●), 49 nm (■), 55 nm (◆), 61 nm (▲), 73 nm (▼) and 171 nm (⊞)) compared to 70% cold rolled Ni (GNB spacing = 280 nm (+)) and 98 % cold rolled Ni (GNB spacing = 133 nm (×)) [42]

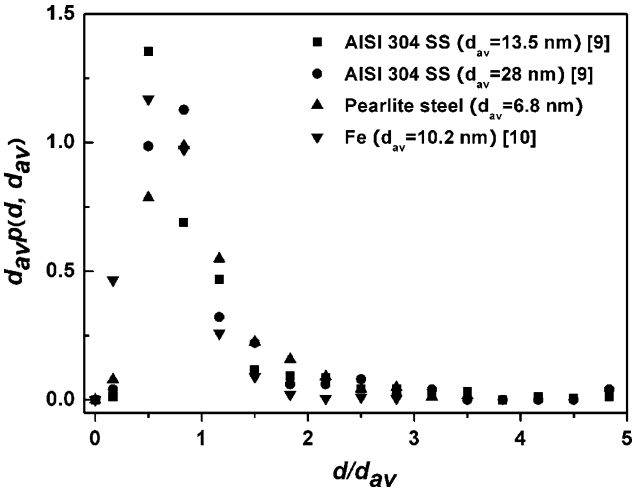

Fig. 13 Probability distributions of nanometer scale boundary spacing normalized by their average spacing in SMAT deformed AISI 304 stainless steel [9], Fe [10] and pearlitic steel (H.W. Zhang et al., unpublished)

deformation induced boundaries and twin boundaries. The dislocations are present in low and medium angle dislocation boundaries and as loose dislocations between the boundaries. Based on these structural features, the dominating strengthening processes are assumed to be: (i) dislocation strengthening with a strength contribution $\Delta\sigma$ (ρ) proportional to $\rho^{1/2}$ where ρ is the dislocation density and (ii) boundary strengthening with a contribution proportional to $D_{\mathrm{HAB}}^{-1/2}$ where D_{HAB} is the spacing between the high angle boundaries which are considered to be impenetrable to moving dislocations. This property characterizes high angle boundaries (>15°) including twin boundaries but it may also be a characteristic of dislocation boundaries having a misorientation angle above a critical values which may be as low as 2–3° [19]. This means that only low angle dislocation boundaries and dislocations between boundaries contribute to $\Delta\sigma$ (ρ), whereas the remaining boundaries contribute to $\Delta\sigma$ (D) The dislocation strengthening has been expressed [19]

$$\Delta\sigma(\rho) = M\alpha Gb\sqrt{\rho_0 + \rho_{\mathrm{LAB}}} \tag{1}$$

where M is the Taylor factor (~3), α is a number of the order of 0.2–0.3, G is the shear modulus and b is Burgers vector, ρ_o is the dislocation density between boundaries and ρ_{LAB} is the dislocation density in low angle boundaries. For a mixed tilt/twist boundary ρ_{LAB} has been expressed [50, 51]

$$\rho_{\mathrm{LAB}} = 1.5(S_v\theta)_{\mathrm{LAB}}/b, \tag{2}$$

where $(S_v\theta)_{\mathrm{LAB}}$ is the boundary area per unit volume and misorientation angle, respectively, of low angle boundaries (<3°). The strength contribution from high angle boundaries is related to the boundary spacing according to the Hall–Petch relationship and can be expressed:

$$\Delta\sigma = K_{\mathrm{HP}}D_{\mathrm{HAB}}^{-1/2} \tag{3}$$

where K_{HP} is a constant which is obtained from the yield stress–grain size relationship of polycrystalline metals [50] see Table 1. On the assumption of a linear additivity of the strength contributions, the total flow stress can be expressed [19, 50, 51]:

$$\sigma = \sigma_0 + M\alpha G\sqrt{1.5b(S_v\theta)_{\mathrm{LAB}}} + K_{\mathrm{HP}}D_{\mathrm{HAB}}^{-1/2} \tag{4}$$

where σ_0 is the friction stress. This analysis emphasizes the importance of both dislocation strengthening and high angle boundary strengthening. Frequently however, the flow stress-structure analysis of nanostructured metals are based on only one structural parameters, the average spacing between all the boundaries (D_B) not considering the character of the boundary or the dislocation density between the

Table 1 Material parameters [50]

Material	G (MPa)	b (nm)	K_1 (MPa m$^{1/2}$)
Aluminum	26,000	0.286	0.04
Nickel	79,000	0.249	0.16
Copper	45,000	0.256	0.14

σ_0 is approximatey 20 MPa for all three metals
K_1 corresponds K_{HP} in this paper

boundaries which can be high [26]. The one parameter equation is expressed [52, 53]:

$$\sigma = \sigma_0 + K_B D_B^{-1/2} \quad (5)$$

By applying Eq. 5 to experimental data a good agreement has been found however with a value of K_B much higher than K_{HP} and also in many cases with a negative value of σ_0. This is shown in Fig. 14, where data for Ni cold rolled over a large strain range are plotted according to Eq. 5 [42]. For comparisons is in Fig. 14 also plotted the stress–grain size relationship for polycrystalline Ni [54], showing a significant smaller slope and a positive value of σ_0.

Equation 4 has been applied with good result for cold rolled Ni [42], Al [46] and IF-steel [55], which at large strain have a structural scale in the range 100–200 nm. For smaller spacings Eq. 4 will be discussed in the following.

For samples with a structural scale <100 nm deformed by HPT, SMAT and sliding most information is obtained for Ni (99.95%) deformed by HPT up to five turns under a uniaxiel pressure of 6 GPa [56]. The deformation structure has been analyzed by TEM and a dislocation density of (5–10) 10^{14} m^{-2} has been reported. No twins and texture have been found. Based on Eq. 1 and Table 1, $\Delta\sigma$ (ρ) is 318–449 MPa. The grain size has been measured to be 105 ± 69 nm and a subgrain size is reported to be 34 nm [56]. Based on Eq. 3 the contribution from grains is 494 MPa and the minimum and maximum value of the flow stress is therefore 812 and 913 MPa, respectively. If the structure is considered be to a subgrain structure Eq. 3 gives a contribution of 868 MPa, and the minimum and maximum value is 1,186 and 1,317 MPa, respectively. These estimated values can be compared with the yield stress and UTS which is 1,000 and 1,270 MPa, respectively [56]. This analysis focuses on the grain size or boundary spacing in the deformed sample, where the structure is found to be equiaxed. This finding relates to the observation plane which is the torsion plane. A characteristic structure of a HPT sample is however obtained in the longitudinal section, see Fig. 5 [14]. This typical structure is subdivided by lamellar boundaries and interconnecting boundaries of varying misorientation angle. This sample section will therefore be used in a future structural analysis to underpin Eq. 4.

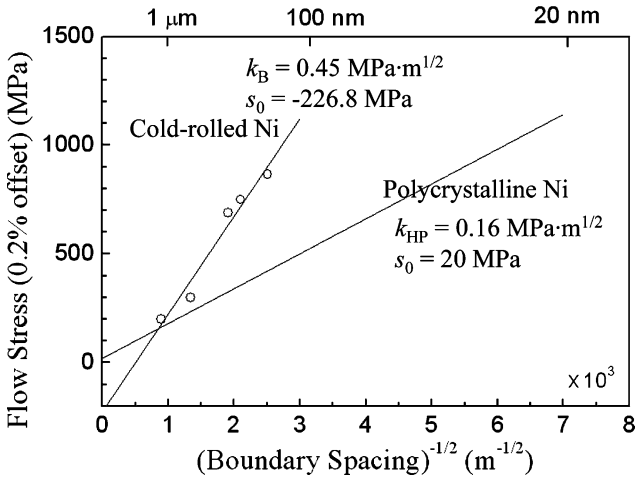

Fig. 14 The flow stress-boundary spacing relationship at room temperature for polycrystalline Ni, and for cold rolled Ni, where K_{HP}, K_B in the figure correspond K_1 and K_2 in Fig. 2 of [50]. The boundary spacing is the grain size for polycrystalline Ni [54] and the boundary spacing along random lines for cold rolled Ni [42]

For specimen deformed by SMAT, very good strength properties have been obtained for example yield strength of 760 MPa for Cu [57] and 1,450 MPa for AISI 316 stainless steel [58]. However, in both studies the microstructural analysis has been limited to a determination of the boundary spacing (grain size) which an average is 30 nm in Cu and 40 nm in AISI 316 stainless steel. However, for both materials a large spreading in boundary spacing (grain size) is observed. Such a large spread has also been found in HPT Ni where grains up to 350 nm in a structure with an average grain size of 105 nm [56]. These findings exemplify the complexity in the quantitative characterization of the microstructures in the deformed nanostructured metals.

Concluding remarks

Deformation by HPT, SMAT and sliding can produce microstructures with a length scale of 5–100 nm. Bulk samples can be produced by HPT, whereas SMAT and sliding results in nanostructured surface layers with a depth of the order of 10–50 μm. All three processes introduce strain gradients resulting in graded microstructures. The microstructure is refined continuously with increasing strain and the subdividing features are dislocation boundaries and high angle boundaries, including grain boundaries, twin boundaries and phase boundaries. For medium and high stacking fault energy metals dislocation processes are dominating down to a structural dimension of 5–10 nm. Additionally, mechanical twins can be formed caused by the high stress required to deform the fine scale metals. Very large flow stress characterizes the nanostructured metals as exemplified by samples deformed by HPT and SMAT. The formulation of strength–structural relationships for these fine scale metals awaits a

detailed identification and quantification of the structural parameters which control the strength.

Acknowledgments We gratefully acknowledge the Danish National Research Foundation for supporting the Center for Fundamental Research: Metal Structures in Four Dimensions, within which this work was performed. The authors also thank X. Huang for helpful discussions.

References

1. Script Mater 51 (2004) 751–841 (Viewpoint Set NO. 35. 'Metals and alloys with a structural scale from the micrometer to the atomic dimension', edited by N. Hansen)
2. Valiev RZ, Islamgaliev RK, Alexandrov IV (2000) Progr Mater Sci 45:103
3. Richert M, Liu Q, Hansen N (1998) Mater Sci Eng 260A:275
4. Saito Y, Tsuji N, Utsunomiya H, Sakai T, Hong RG (1998) Scripta Mater 39:1221
5. Hughes DA, Hansen N (2001) Phys Rev Lett 87:135503
6. Fecht HJ, Hellstern E, Fu Z, Johnson WL (1990) Metall Trans 21A:2333
7. Umemoto M, Todaka Y, Tsuchiya K (2003) Mater Trans 44:1488
8. Lu K, Lu J (1999) J Mater Sci Technol 15:193; Mater Sci Eng (2004) 375–377A:38
9. Zhang HW, Hei ZK, Liu G, Lu J, Lu K (2003) Acta Mater 51:1871
10. Tao NR, Wang ZB, Tong WP, Sui ML, Lu J, Lu K (2002) Acta Mater 50:4063
11. Wu X, Tao N, Hong Y, Xu B, Lu J, Lu K (2002) Acta Mater 50:2075
12. Zhu KY, Vassel A, Brisset F, Lu J, Lu K (2004) Acta Mater 52:4101
13. Scripta Mater. 49 (2003) 625–680 (Viewpoint Set No. 31. 'Mechanical properties of fully dense nanocrystalline metals', edited by H. Van Swygenhoven and J.R. Weertman)
14. Huang X, Vorhauer A, Winther G, Hansen N, Pippan R, Zehetbauer M (2004) In: Zhu YT, Langdon TG, Valiev RZ, Semiatin SL, Shin DH, Lowe TC (eds) Ultrafine grained materials III. TMS (The Minerals, Metals & Materials Society), p 235
15. Huang X, Winther G, Hansen N, Hebesberger T, Vorhauer A, Pippan R, Zehetbauer M (2003) Mater Sci Forum 426–432:2819
16. Winther G, Hansen N, Hebesberger T, Huang X, Pippan R, Zehetbauer M (2001) In: Dinesen AR, Eldrup M, Juul Jensen D, Linderoth S, Pedersen TB, Pryds NH, Schrøder Pedersen A, Wert JA (eds) Proceedings of the 22nd Risø international symposium on materials science: science of metastable and nanocrystalline alloys-structure, properties and modeling, Risø National Laboratory, Roskilde, Denmark, p 435
17. Zhilyaev AP, Lee S, Nurislamova GV, Valiev RZ, Landon TG (2001) Scripta Mater 44:2753
18. Hughes DA, Dawson DB, Korellis JS, Weingarten LI (1995) Wear 181:458
19. Hansen N (2004) In: Gundlach C, Haldrup K, Hansen N, Huang X, Juul Jensen D, Leffers T, Li ZJ, Nielsen SF, Pantleon W, Wert JA, Winther G (eds) Proceedings of the 25th Risø international symposium on materials science: evolution of deformation microstructures in 3D. Risø National Laboratory, Roskilde, Denmark, p 13
20. Huang X, Tsuji N, Hansen N, Minamino Y (2003) Mater Sci Eng 340A:265
21. Hughes DA, Hansen N (2004) ASM handbook 10th edn., vol 9: metallography and microstructures. ASM International, Metals Park, Ohio, p 192
22. Kuhlmann-Wilsdorf D, Hansen N (1991) Scripta Metall Mater 25:1557
23. Kuhlmann-Wilsdorf D (1989) Mater Sci Eng 113A:1
24. Kuhlmann-Wilsdorf D (1985) Phys Stat Sol 225:225
25. Liu Q, Hansen N (1995) Scripta Metall Mater 32:1289
26. Hughes DA, Hansen N (2003) Phil Mag 83:3871
27. Bay B, Hansen N, Hughes DA, Kuhlmann-Wilsdorf D (1992) Acta Metall Mater 40:205
28. Hansen N (2001) Metall Mater Trans 32A:2917
29. Zhilyaev AP, Kim B-K, Nurislamova GV, Baró MD, Szpunar JA, Langdon TG (2002) Scripta Mater 46:575
30. Honeycombe RWK (1984) The plastic deformation of metals. Edward Arnold Ltd
31. Liao XZ, Zhou F, Lavernia EJ, He DW, Zhu YT (2003) Appl Phys Lett 83:5062
32. Rösner H, Markmann J, Weissmüller J (2004) Phil Mag Lett 84:321
33. Chen MW, Ma E, Hemker KJ, Sheng HW, Wang YM, Cheng XM (2003) Science 300:1275
34. Liao XZ, Huang JY, Zhu YT, Zhou F, Lavernia EJ (2003) Philos Mag 83:3065
35. Asaro RJ, Krysl P, Kad B (2003) Philos Mag Lett 83:733
36. Zhu YT, Liao XZ, Srinivasan SG, Zhao YH, Baskes MI, Zhou F, Lavernia EJ (2004) Appl Phys Lett 85:5049
37. Zhu YT, Liao XZ, Srinivasan SG, Lavernia EJ (2005) J Appl Phys 98:034319
38. Van Swygenhoven H, Derlet PM, Frøseth AG (2004) Nature Mater 3:399
39. Yamakov V, Wolf D, Phillpot SR, Mukherjee AK, Gleiter H (2004) Nature Mater 3:43
40. Schiøtz J, Di Tolla FD, Jacobsen KW (1998) Nature 391:561
41. Schiøtz J, Jacobsen KW (2003) Science 301:1357
42. Hughes DA, Hansen N (2000) Acta Mater 48:2985
43. Alberdi J (1984) Universidad de Navarra Facultad de Ciencias, San Sebastian, Grandes Deformaciones Plasticas en Frio en Policristales de Cobrey Aluminio (Torsion)
44. Hu H (1969) In: Grewen J, Wassermann G (eds) Textures in research and practice. Springer-Verlag, Berlin, p 200
45. Dinda GP, Rösner H, Wilde G (2005) Scripta Mater 52:577
46. Liu Q, Huang X, Lloyd DJ, Hansen N (2002) Acta Mater 50:3789
47. Godfrey A, Hughes DA (2002) Mater Character 48:89
48. Hughes DA, Chrzan DC, Liu Q, Hansen N (1998) Phys Rev Lett 81:4664
49. Godfrey A, Hughes DA (2004) Scripta Mater 51:831
50. Hansen N (2004) Scripta Mater 51:801
51. Hansen N, Huang X, Ueji R, Tsuji N (2004) Mater Sci Eng 387–389A:191
52. Hall EO (1951) Proc Phys Soc London 64B:747
53. Petch NJ (1953) J Iron Steel Inst 174:25
54. Thompson AAW (1975) Acta Metall 23:1337
55. Li BL, Godfrey A, Meng QC, Liu Q, Hansen N (2004) Acta Mater 52:1069
56. Dalla Torre F, Spätig P, Schäublin R, Victoria M (2005) Acta Mater 53:2337
57. Wang YM, Wang K, Pan D, Lu K, Hemker KJ, Ma E (2003) Scripta Mater 48:1581
58. Chen XH, Lu J, Lu L, Lu K (2005) Scripta Mater 52:1039